Magnetic Induction of Conductive Nanosprings

A Thesis
Presented in Partial Fulfillment of the Requirements for the
Degree of Master of Science
with a
Major in Physics
in the
College of Graduate Studies
University of Idaho

by
Marshall Boyland

Major Professor: Andreas E. Vasdekis, Ph.D.
Committee Members: David N. McIlroy, Ph.D.; Brian K. Johnson, Ph.D.
Administrator: Ray von Wandruszka, Ph.D.

May 2018

Authorization to Submit Thesis

This thesis of Marshall Boyland, submitted for the degree of Master of Science with a Major in Physics and titled “Magnetic Induction of Conductive Nanosprings,” has been reviewed in final form. Permission, as indicated by the signatures and dates below, is now granted to submit final copies to the College of Graduate Studies for approval.

Major Professor: _____ Date: _____

Andreas E. Vasdekis, Ph.D.

Committee Members: _____ Date: _____

David N. McIlroy, Ph.D.

_____ Date: _____

Brian K. Johnson, Ph.D.

Administration: _____ Date: _____

Ray von Wandruszka, Ph.D.

Abstract

Nanosprings grown on a substrate produce a 3D network of randomly connected microscopic springs. The springs are made of silicon dioxide on the order of 10 nm in diameter. The motion of electrical current through the 3D network of nanosprings is of interest for the integration of nanosprings into electronic devices. To make the nanosprings conductive they are coated in graphene by a process called Graphite from the University of Idaho Thermolyzed Asphalt Reaction (GUITAR). The following data demonstrate the equipment configuration necessary to obtain a low noise signal to investigate the electrical response of GUITAR coated nanosprings due to magnetic flux. When comparing the response of a sample of nanosprings to a comparable resistor it was found that the nanospring sample is more sensitive to smaller magnetic flux than to larger magnetic flux.

Acknowledgements

I would like to express my deepest gratitude to David McIlroy for welcoming me into his research group and providing me with a challenging, yet enjoyable research experience. He provided an excellent balance between independent work and “hand holding” assistance (though, not without a healthy amount of banter) as I progressed with my project and could not be happier with the education I received.

Additionally, I want to thank John Failla, without whom this project would not have been possible. He is an incredibly talented machinist who is very professional and a pleasure to work with. Also a big thanks to Negar Rajabi, who assisted me in numerous vital lab procedures that allowed me to prepare the samples I needed in order to complete my project. She demonstrated great patience when I was in need of recurring assistance with lab equipment.

Dedication

I would not be where I am today if it had not been for my incredibly supportive parents, Michael and Charlotte. They have always encouraged me to push myself and I would not have been able to do this project without the work ethic and values they instilled in me.

Lastly, I want to thank my wonderful wife, Gabriela for initially encouraging me to attend graduate school and by supporting me through my stresses, late nights, and weekends on campus. I am blessed to have been able to earn my degree with her.

Table of Contents

List of Figures

1. Introduction

Nanowires have received increased attention due to their diverse electrical, optical, and mechanical properties (Zhang et al.). A subset of nanowires include nanosprings which have many applications in areas such as orthopedic bonding devices (Hass et al.), microreactors (Schilke et al.), and olfactory sensors (Dobrokhotov et al.). The scope of this project is much more broad. It specifically looks at the magnetic inductance and current paths of a mat (~1 cm^2) of silicon dioxide (SiO_2) nanosprings that have been treated with Graphite material from the University of Idaho Thermolyzed Asphalt Reaction (GUITAR) (Cheng et al.).

Nanosprings are microscopic silicon dioxide wires that, when grown, coil in a helical shape. They create a 3-D array of nanosprings that are ~60 nm in diameter and ~1 µm in length (McIlroy et al.) (figure 1.1) and are formed via the vapor-liquid-solid mechanism (Wagner and Ellis). The helical growth pattern has been described by several mechanisms. The first of which investigates the contact angle anisotropy of a catalyst droplet at the catalyst/nanowire interface which causes an asymmetry of the growth front velocity for the nanosprings (McIlroy et al.). This results in the helical growth pattern that can be seen in figure 1.2. The second explanation is that a temperature gradient from the core of the nanowire to the surface will cause a gradient in the growth rate which results in the aforementioned helical growth (Zhang et al.). The current model focuses on oxygen diffusion. The outer part of the nanowire inhibits oxygen diffusion in the middle which causes the necessary growth gradient to result in the helical morphology (Wojcik et al.). Figure 1.3 nicely demonstrates the multi-nanowire morphology.

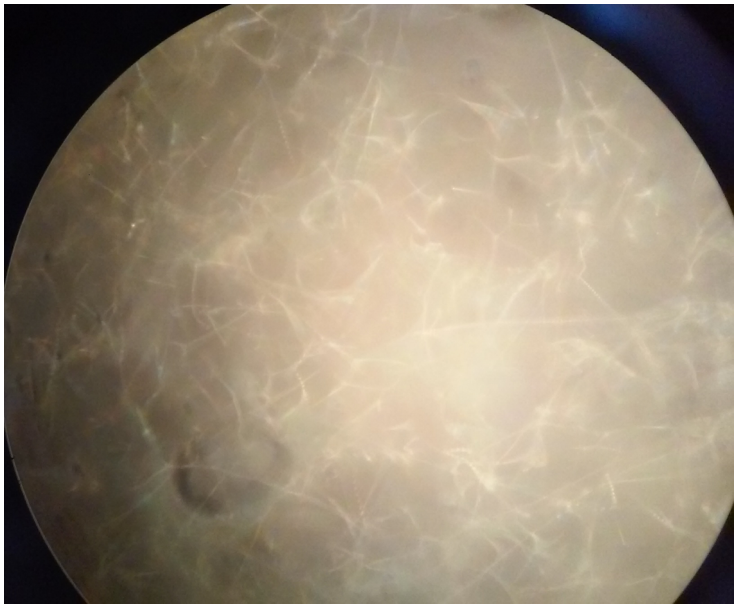

Figure 1.1 Silicon dioxide nanospring sample at 400X magnification.

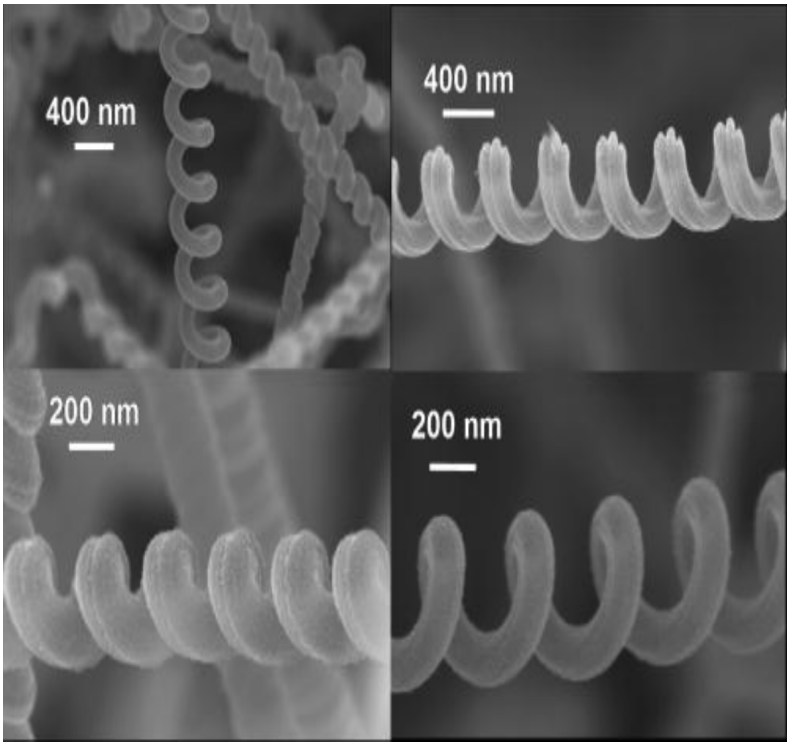

Figure 1.2 SEM of silicon dioxide nanospring helical growth.

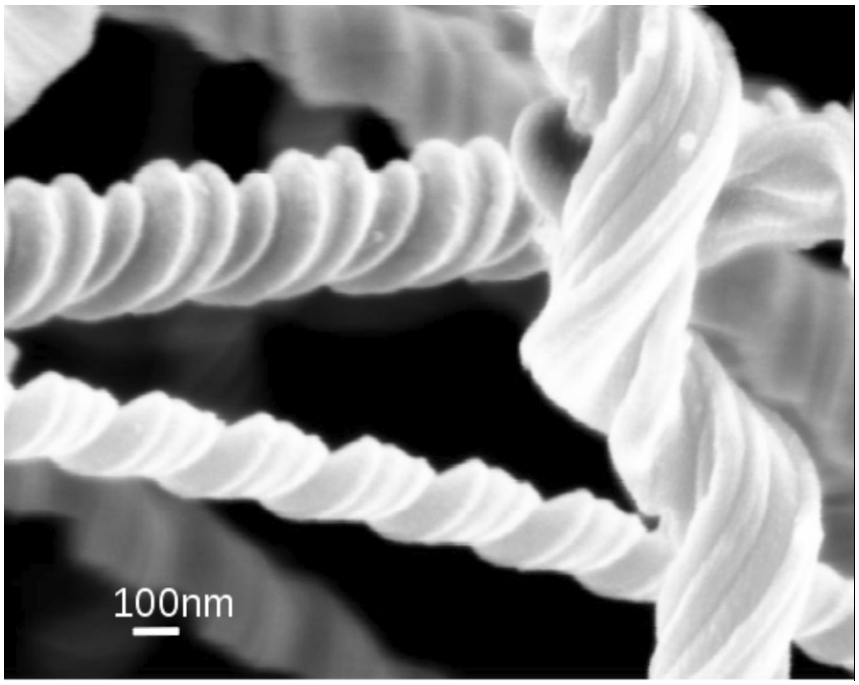

Figure 1.3 SEM of silicon dioxide nanospring multiwire morphology.

Work with nano networks has mostly focused on manufacturing or treatment techniques to increase electrical performance (Tan et al.; Bao et al.; Gao and Gu; Sun et al.). Another focus with nano networks is investigating the percolation threshold density; the minimum network density at which conduction occurs. The most fundamental investigation of the percolation threshold was done by a group from the University of California Los Angeles in 2004. Hu et al. measured the conductance and optical transmittance of sheets of single-walled carbon nanotube networks at different nanotube network densities. Their findings for conductivity fit well with the 2-D percolation threshold predicted from percolation theory and the optical transmittance agreed broadly with previous work. Research is also being conducted to decrease the percolation threshold of nano networks. This has been done by introducing Ag fillers to the nano network (Zulkarnain et al.), doping with insulative B_2O_3 (Ulrich et al.), and introducing nano-engineered networks of a non-conductive and semi-conductive polymers (Barbero et al.).

This project is the first step into investigating the percolation threshold of induction i.e., what size (or threshold) of a nanospring network will cut off all current loops. It will also provide insightful information as to how charge carriers behave in electrical devices such as

remote sensors and solar panels. Additionally, this research can be utilized when integrating nanosprings into nanowire technology such as the previously mentioned examples.

2. Characterization/Theory

Moving charges interact with magnetic fields according to the Lorentz Force Law. This law states that a charge moving in a magnetic field will experience a force perpendicular to its velocity and the magnetic field. Mathematically this is represented as:

$$\vec{F} = Q(\vec{E} + (\vec{v} \times \vec{B}))$$

where Q is the charge, E is the electric field, v is velocity and B is the magnetic field (Griffiths, "The Lorentz Force Law"). This is the basis for magnetic induction, which is stimulating a current in a conductive material using a changing external magnetic field.

Magnetic induction can be quantified by Faraday's Law which states that a conductive material in the presence of a changing external magnetic field will manifest an electric field within the material and thus, produce an electrical current. This law is represented mathematically as:

$$\vec{\nabla} \times \vec{E} = -\frac{\partial \vec{B}}{\partial t}$$

Another form of this law can be written as $\varepsilon = -\frac{d\phi}{dt}$ (Griffiths, "Electromagnetic Induction"), where ε is the EMF and ϕ is the magnetic flux through a loop. The latter of which is the more useful form for this experiment. Nanospring samples contain a plethora of interconnected loops with a constant resistance that form electrical connections and contribute to magnetic induction. By minimizing the sample geometry, it is possible to find the minimum loop size at which nanosprings form and/or allow induction.

3. Experimental Techniques

3.1. Material Preparation and Growth

For this experiment, all substrates were thoroughly cleaned using acetone, isopropyl alcohol, and deionized water before any treatment. The nanosprings were grown for 60 minutes on a quartz substrate ~1 cm^2 that had been pretreated with silicon dioxide in the growth chamber (figures 3.1 and 3.2) for 30 minutes with a 20 second Au sputter.

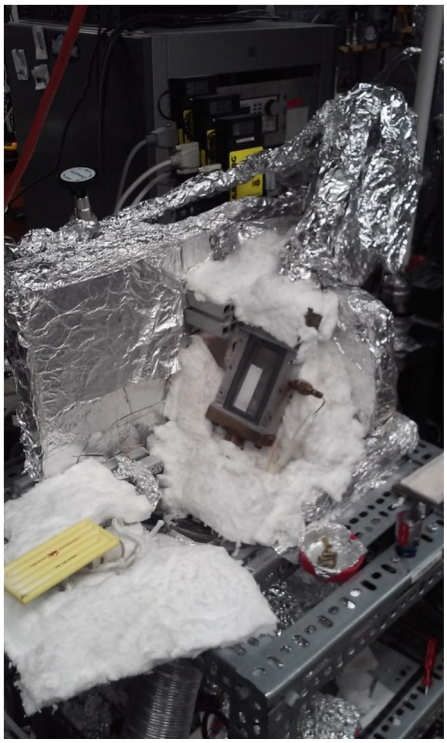

Figure 3.1 Inside of small nanospring chamber.

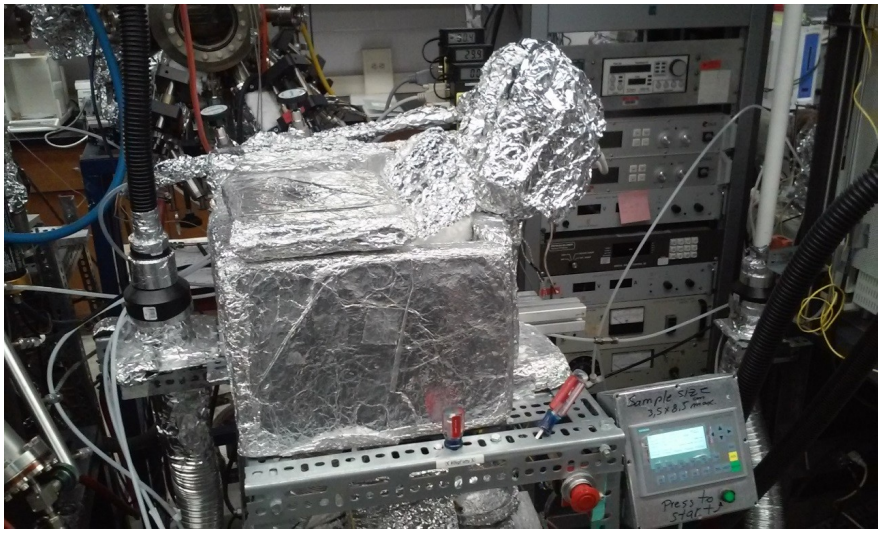

Figure 3.2 Small nanospring chamber during growth.

Made of silica, nanosprings are insulative so they must be coated in GUITAR to become conductive (figure 3.3). From this process, the resistance of a nanospring sample can be reduced to ~10 Ω. They were coated in GUITAR for approximately 60 minutes which resulted in resistances between 50 Ω and 5 kΩ.

Figure 3.3 GUITAR coating chamber.

The GUITAR process uses the vapor of a sulfur and cyclohexanol, $C_6H_{12}O$ mixture. The solution is heated in the beaker (on the left of figure 3.3) while N_2 flows through the solution and into the tube furnace. As the mixture evaporates, the vapor is passed via the N_2 into the furnace where the sample is heated for coating. The vapor deposits carbon conformally throughout the sample such that all surfaces of the nanosprings are coated with the conductive carbon (figure 3.4).

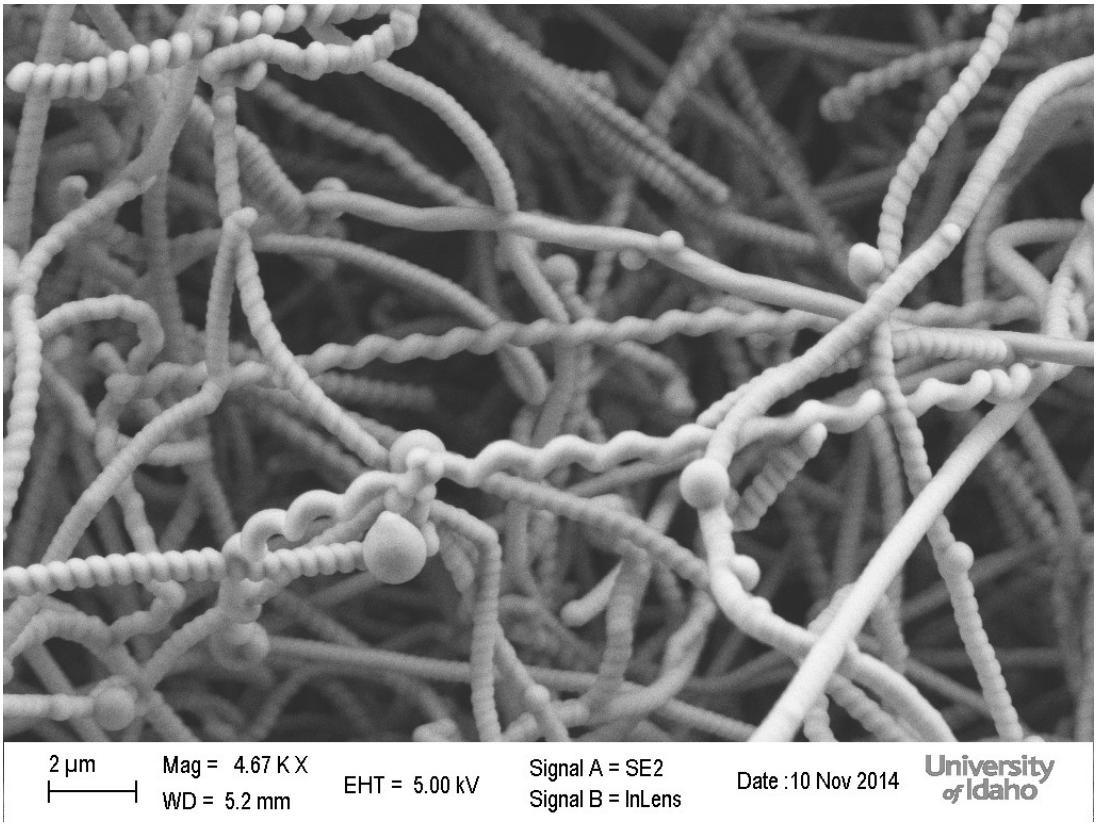

Figure 3.4 SEM of nanospring sample after GUITAR coating.

The tested samples consisted of a matted nanospring sample that covered the whole substrate (ns16) (~50 Ω), a nanospring sample that was grown in the shape of a "U" (u21) (~5 kΩ), a quartz substrate coated only in GUITAR as control (cs23) (~500 Ω), and a 500 Ω resistor (500R). Due to comparable surface area and lack of nanosprings, cs23 would act as the control when comparing it to ns16 and 500R. u21 was grown using the same method as ns16 with one exception; after the 30 minute pretreatment, a stainless steel "U" shaped mask

(figure 3.5) was fastened to the front of the sample. This created a “U” shaped Au trace after sputtering. The sample was grown in the same chamber but with an extension cap to make extra space for the mask. The mask is 1 mm in width, which is the smallest width attainable through machining.

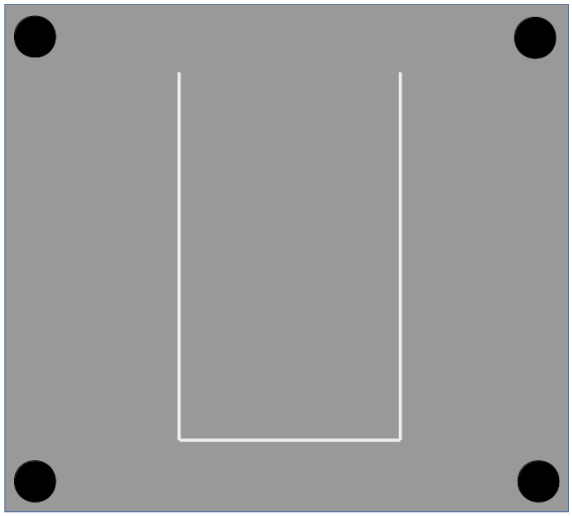

Figure 3.5 “U” shaped mask.

3.2 Instrumentation Design

Trial 1 - The first configuration was set up using:

- Ammeter
- Gaussmeter
- Power supply
- Helmholtz coil
- Computer with GPIB to control the instruments

The equipment was controlled through GPIB using Python (figure 3.6). This design was meant to test two scenarios:

- Measure voltage vs. current with a set external magnetic field
- Measure magnetic field vs. current with a set voltage

The first scenario worked by setting a specific magnetic field with the Helmholtz coil, scanning a range of voltages across the sample at that specific magnetic field, then measuring the current through the sample at each voltage. The second scenario worked by setting a specific voltage across the sample, scanning a range of magnetic fields, then measuring the current through the sample at each magnetic field. Examples of these data can be seen in section 4.1 (figures 4.1 and 4.2).

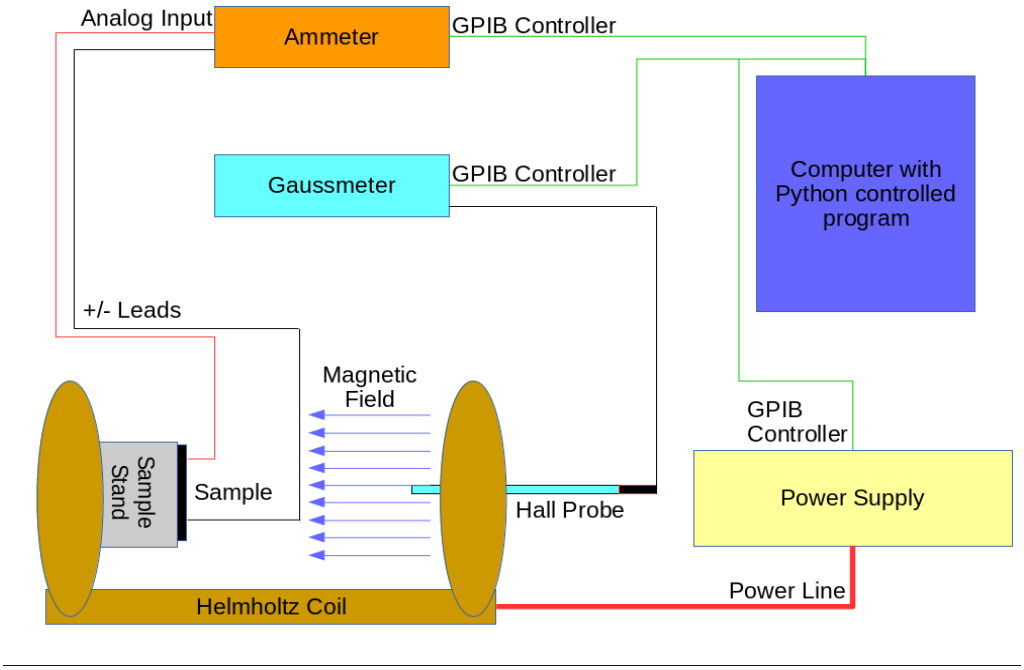

Figure 3.6 Trial 1 schematic.

Trial 2 - A motor controlled by a variac was outfitted with a steel turn table on its axis which held a neodymium magnet with a strength of ~5 kG (at the surface) near the edge. A Teflon stand was used to hold a glass slide over the location on the turn table that held the magnet. The sample was then secured on the glass slide above the turn table (figure 3.9).

Instead of automating the data-taking process, data was taken using the analog output of the ammeter through a DATAQ data acquisition DI-510 device which has a sample rate of 4800 samples/second. This was then connected to the computer via USB. A real time display

from the DATAQ software could be used to see the response from the nanosprings due to the magnetic flux of the rotating magnet.

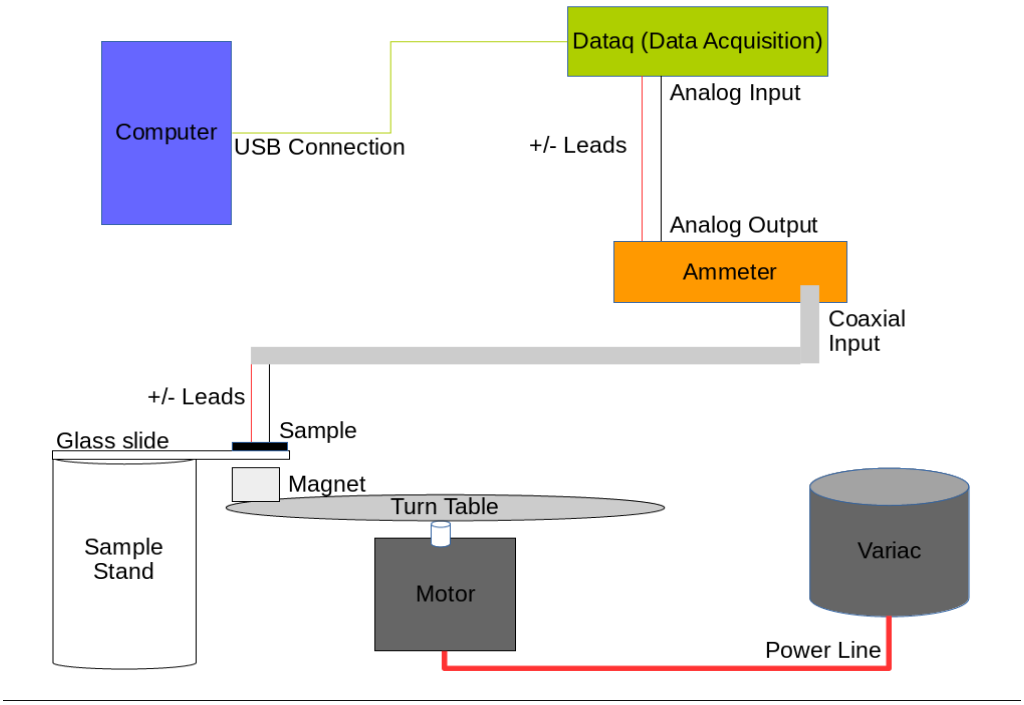

Figure 3.7 Trial 2 schematic.

Trial 3 - The premise was the same as trial 2; using motion relative to a magnetic field to induce a current in the sample. The main difference was that in trial 3, the sample was rotating on the turn table, the magnetic field was stationary, and much more concentrated than the previous design. Other modifications were done to greatly reduce noise from the previous trial:

- A Faraday cage was constructed to contain the sample, magnet casing, motor, and turn table (figure 3.10)
- The leads from the sample were braided and connected to a coaxial cable before exiting the Faraday cage
- All power lines were stripped of their outer casing, braided, and wrapped in grounded Al foil, even wires outside the Faraday cage

The Teflon stand was modified to hold a U-bracket magnet casing and the turn table was made from plexiglass as opposed to steel to avoid magnetic interaction. Other than these changes, the remaining connections are the same as trial 2; the sample connects to the ammeter through a coaxial cable, the analog output of the ammeter connects to the data acquisition which then connects to the computer through USB.

The U-bracket magnet casing is designed to funnel the magnetic field through the casing to limit fringe fields that interfere with the sample as it passes by the magnet. This was achieved by using two pyramid magnets, one north pole and one south pole. They were positioned such that the tips of the pyramids were pointed towards each other to localize the magnetic field (figure 3.10). When separated 0.6 cm the strength of these magnets at the surface of the pyramid was ~9 kG and near the location where the sample rotated was ~ 6 kG. The U-bracket could also be adjusted to vary the distance between the magnets using spacers (~0.6 cm thick); which allowed the strength and shape of the magnetic field to be altered. Another difference with the design included an additional, smaller magnetic field (order ~10 G) from the motor. Since the sample was rotating relative to the motor, the smaller field was detected as opposed to trial 2.

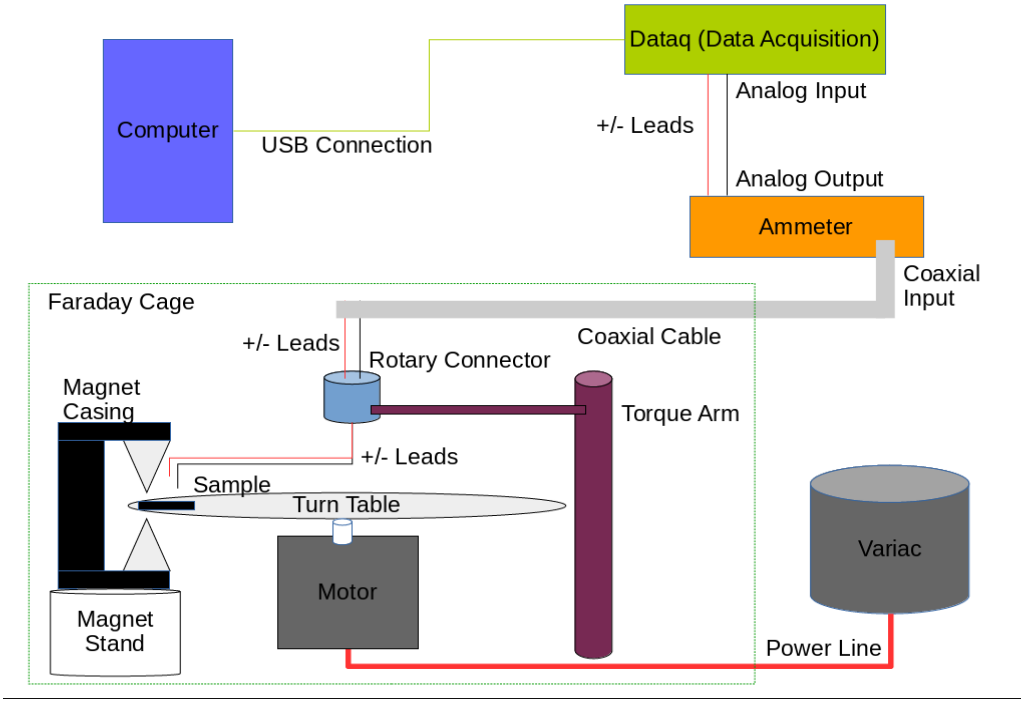

Figure 3.8 Trial 3 schematic.

4. Results

4.1 Trial Results

Trial 1 - This experimental design focused on measuring magneto-resistivity more so than electrical response to magnetic flux. Examples from the results of these tests can be seen in figures 4.1 and 4.2. The data demonstrated that the presence of a magnetic field (strength of the order ~0.5 kG) had no effect on the current being driven through a nanospring sample. The only curious result came from an equipment limitation that appeared as though the current “turned off” at a certain combination of magnetic field and voltage (figure 4.3). The true reason for the anomaly is that after a certain magnetic field strength and current combination, the ammeter would only output the previous measurement, which resulted in the flattening of the plot.

This set up proved to be a slow means of measurement because only one datum was recorded at each specified magnetic field and voltage. To see the full electrical response a much faster measurement would need to be taken.

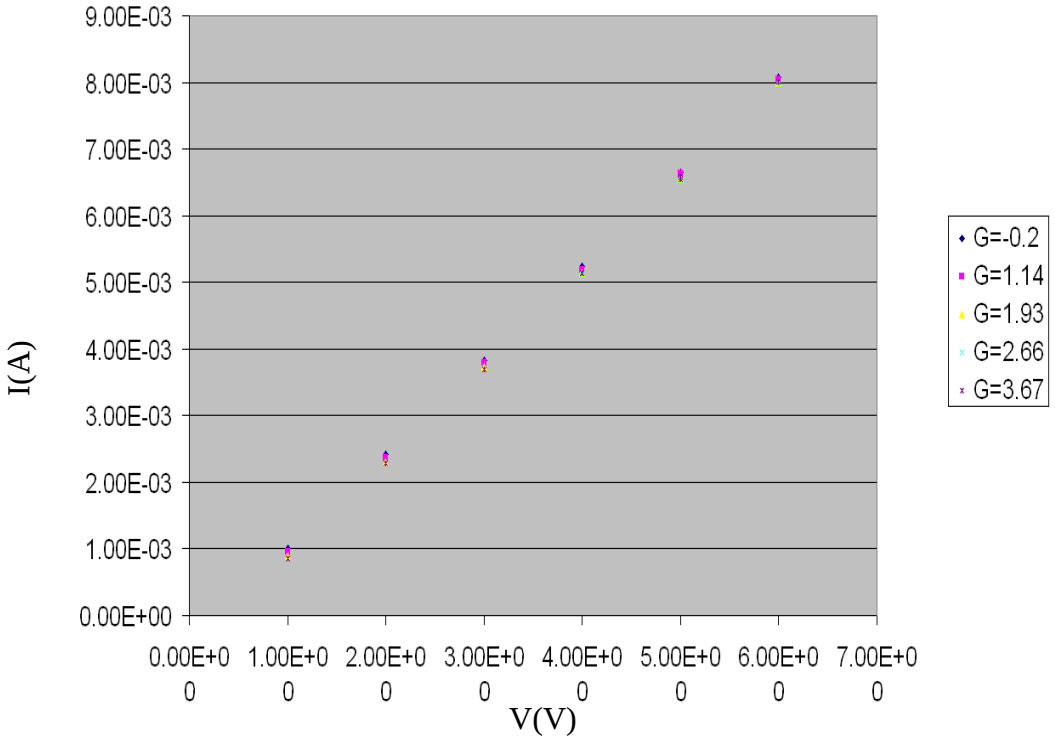

Figure 4.1 Set magnetic field with scanned voltages measurement.

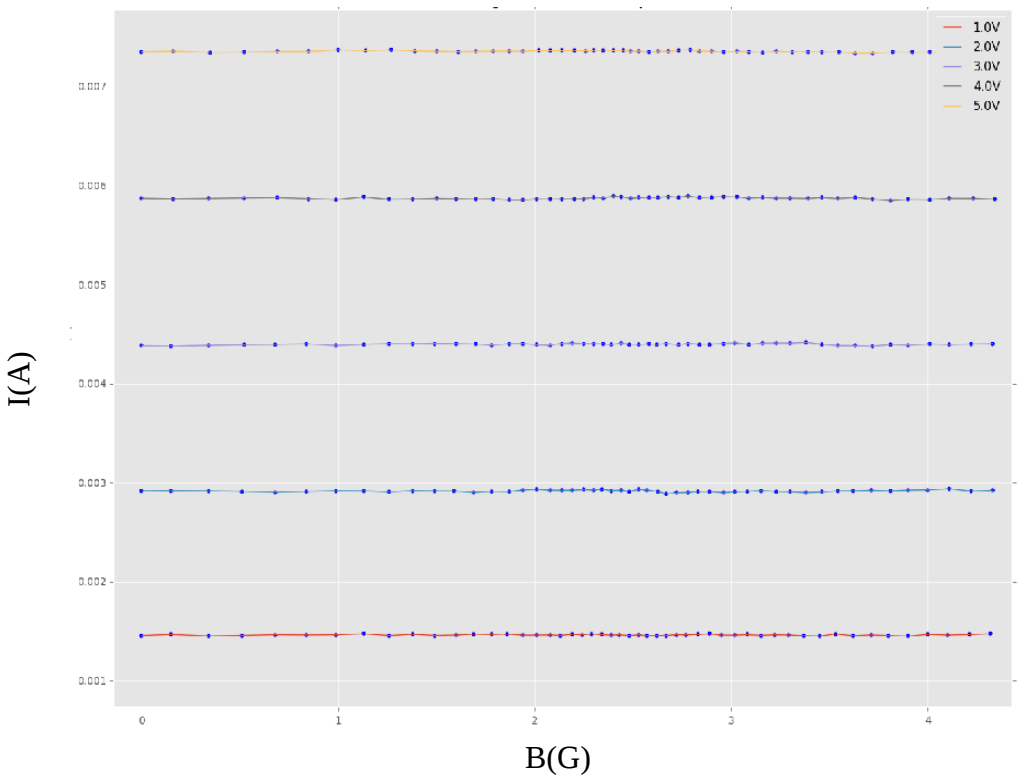

Figure 4.2 Set voltage with scanned magnetic fields measurement.

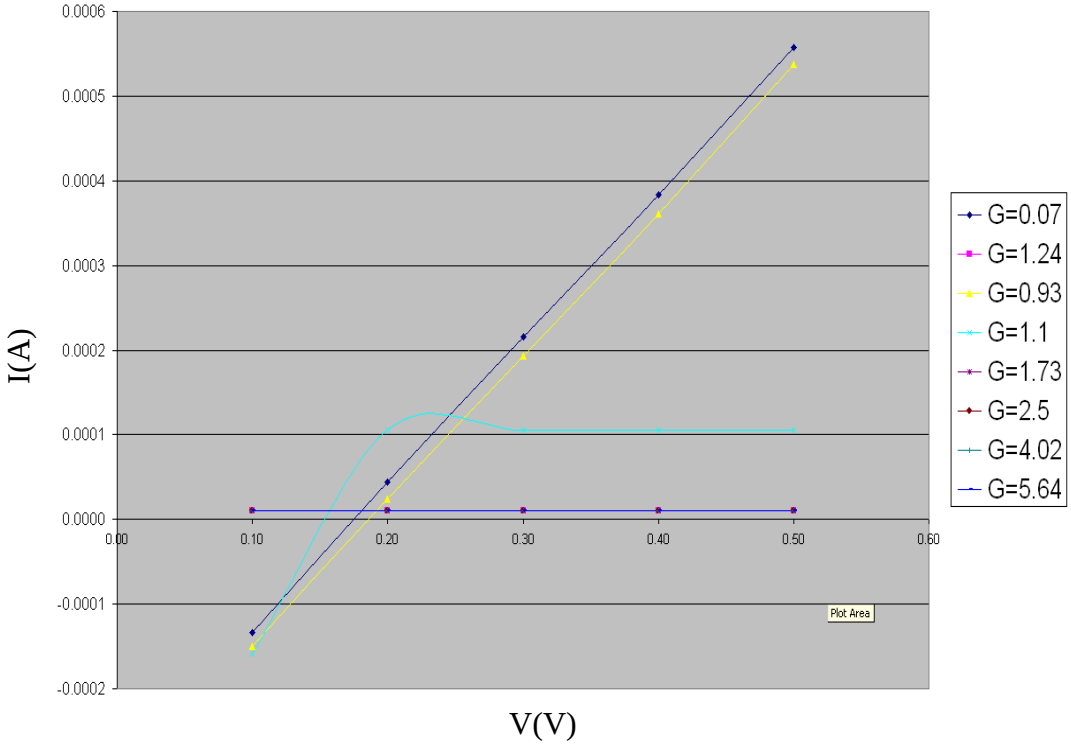

Figure 4.3 Anomaly from equipment limitation.

Trial 2 - Due to the slow measurement design of Trial 1 a much different approach was used for Trial 2. It was indeed a very fast measurement, operating at 4800 samples/second, it recorded and displayed the data in real time. One large problem with this experimental design was the presence of a 60 Hz signal. This signal was from outside sources such as the motor and lights. It was visible in all the data sets, but most prevalent in a fully coated nanospring sample (figure 4.2).

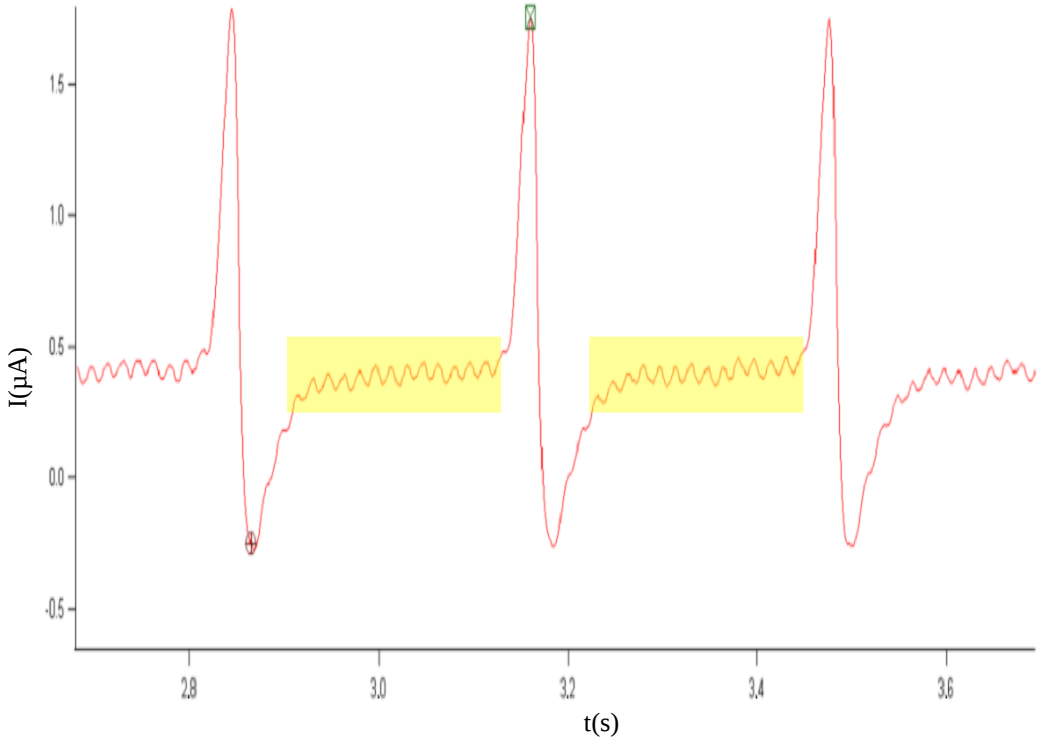

Figure 4.4 Presence of 60 Hz signal in a fully coated nanospring sample.

Trial 3 - The final design was very similar to trial 2 but with the goal of reducing the 60 Hz signal that plagued the data from trial 2. Thanks to the addition of the Faraday Cage, braided wires, and grounded Al shielding, this design excelled in reducing the noise as shown in figure 4.3. The noise, however, is not completely gone but has a very small signal to noise ratio (SNR). The SNR was calculated by averaging the four largest displacements between impulses relative to the small and large magnetic signal. They are calculated to be ~17 and ~238 for the small and large magnetic signals, respectively. Figure 4.4 demonstrates the cyclic signals that were used in the calculation.

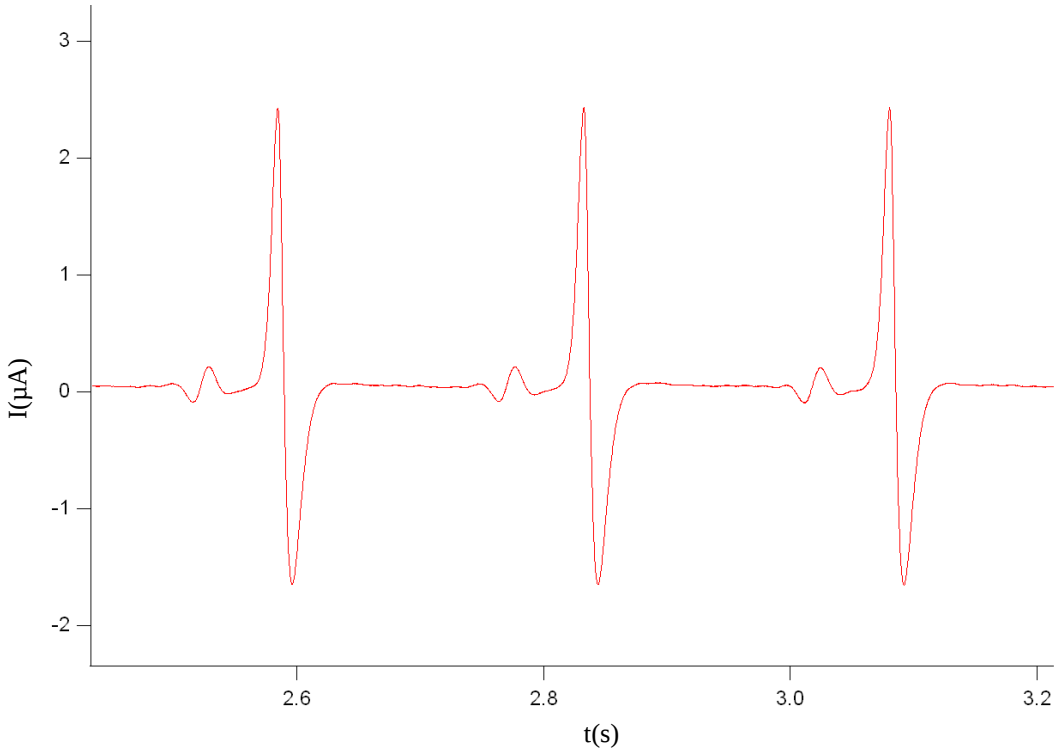

Figure 4.5 Reduction of 60 Hz signal in NS.

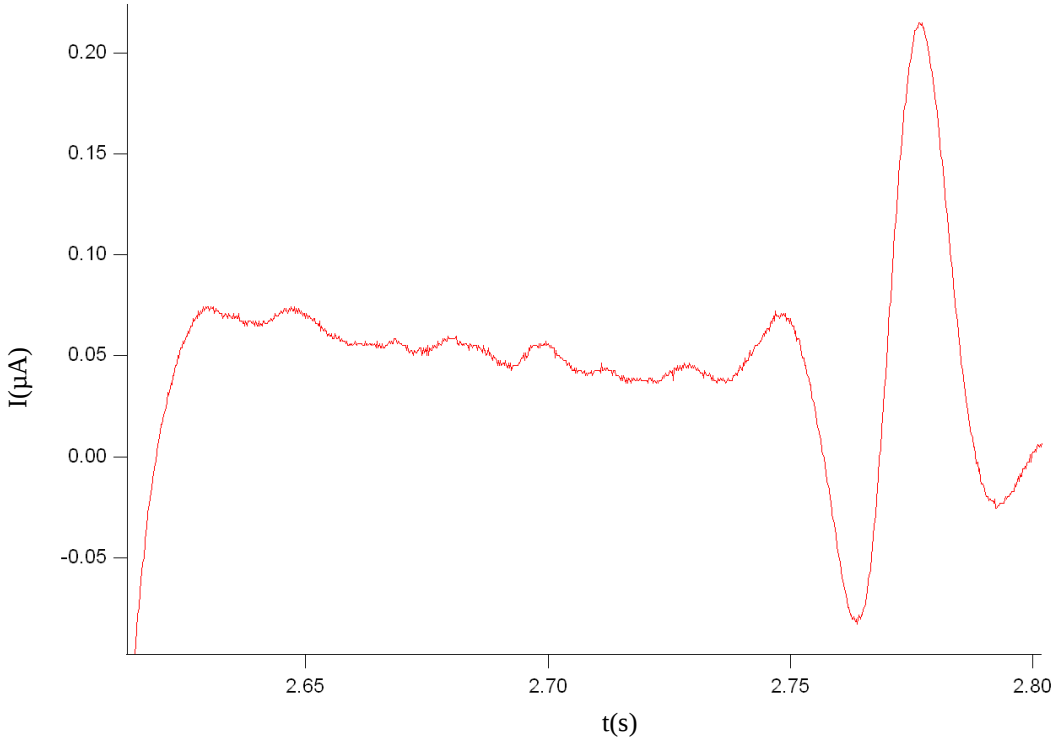

Figure 4.6 Visual of the signal to noise ratio in NS.

When comparing cs23 to 500R, there was little to no difference in the electrical response between the two. The surface of the cs23 samples were very fragile and difficult to use for more than one measurement. Due to the cs23 samples fragility, unspecified resistances, and the fact that they behave nearly identically to a resistor with comparable resistance, resistors were used for most of the comparisons. The same was also true when comparing u21 to ns16, they had nearly identical profiles and the induced current scaled almost perfectly given the differences in resistance (figure 4.5).

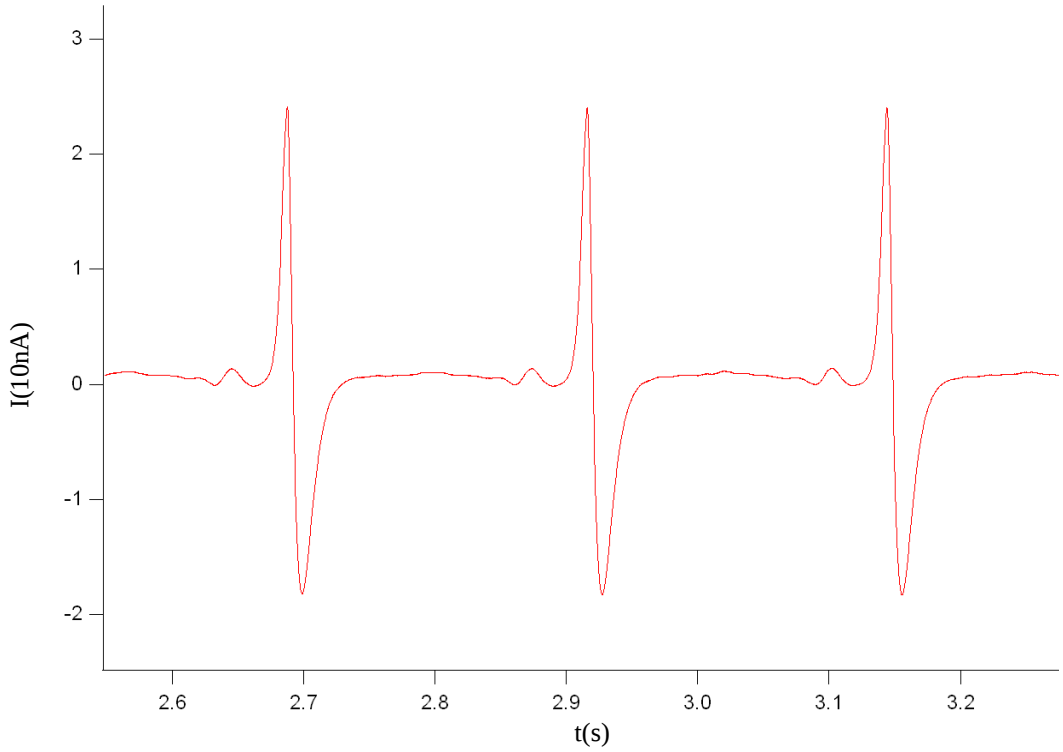

Figure 4.7 Current induced in U.

4.2 Amplitude Ratio

For further analysis, the smaller induced current from the motor was compared to the amplitude of the larger induced current from the magnets. This was done by dividing the peak to peak separation of the smaller signal to the peak to peak separation of the larger signal. This information demonstrates which samples are more sensitive to smaller magnetic fields. To do this, the amplitude ratio (AR) was plotted vs. the tangential speed of the sample.

The AR stayed relatively constant with different tangential speeds with one exception. When compared across samples, ns16 had the largest AR, followed by u21, then 500R, This can be seen in Figure 4.6. Comparing the AR over all rotation speeds followed the same trend. Figure 4.7 demonstrates one very distinct datum with the "Spacer = 6" data set. It has a very large AR for cs23 across all rotation speeds.

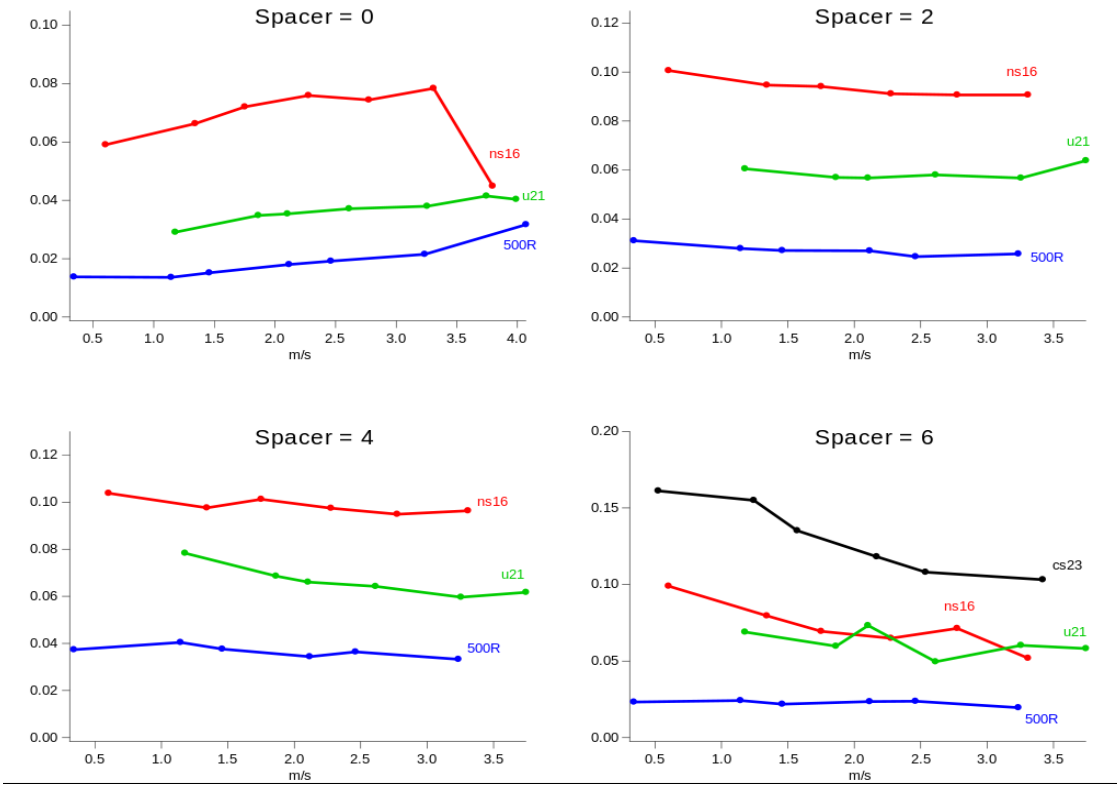

Figure 4.8 Amplitude Ratio comparisons across tangential speeds.

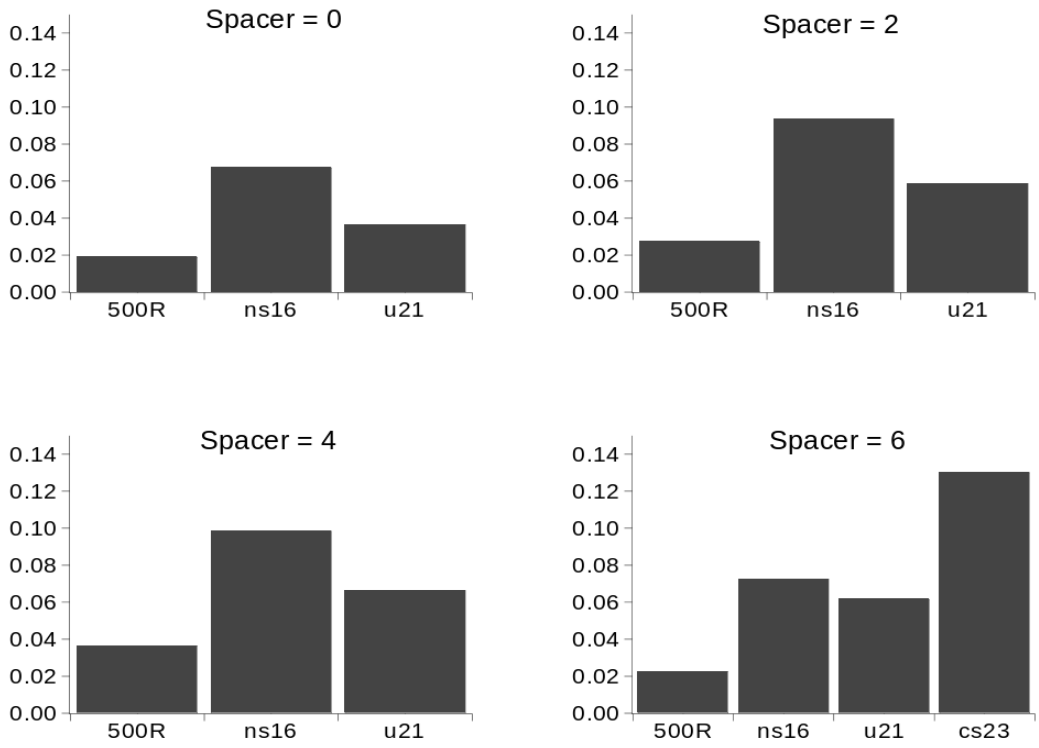

Figure 4.9 Average Amplitude Ratio over all rotation speeds.

To investigate the possibility of a nonzero background current change in the samples a linear regression line was fit to the data. The slope of this line would indicate if the baseline current was changing over time. For data sets with the largest range setting, the largest slope was between $10^{-5} – 10^{-3}$ relative to the vertical axis units, indicating little to no background current changes for the tested tangential velocities.

4.3 Relaxation Time

Another attribute that was investigated is the time taken for the peak induced current to relax back to the zero induction point of the signal. This measurement is referred to as relaxation time (RT). This was measured by using the intersection of the relaxed signal between impulses and the linear fit line from the end of section 4.2. The RT is hypothesized to be greater in the samples with nanosprings due to the finite number of current paths available to the electrons.

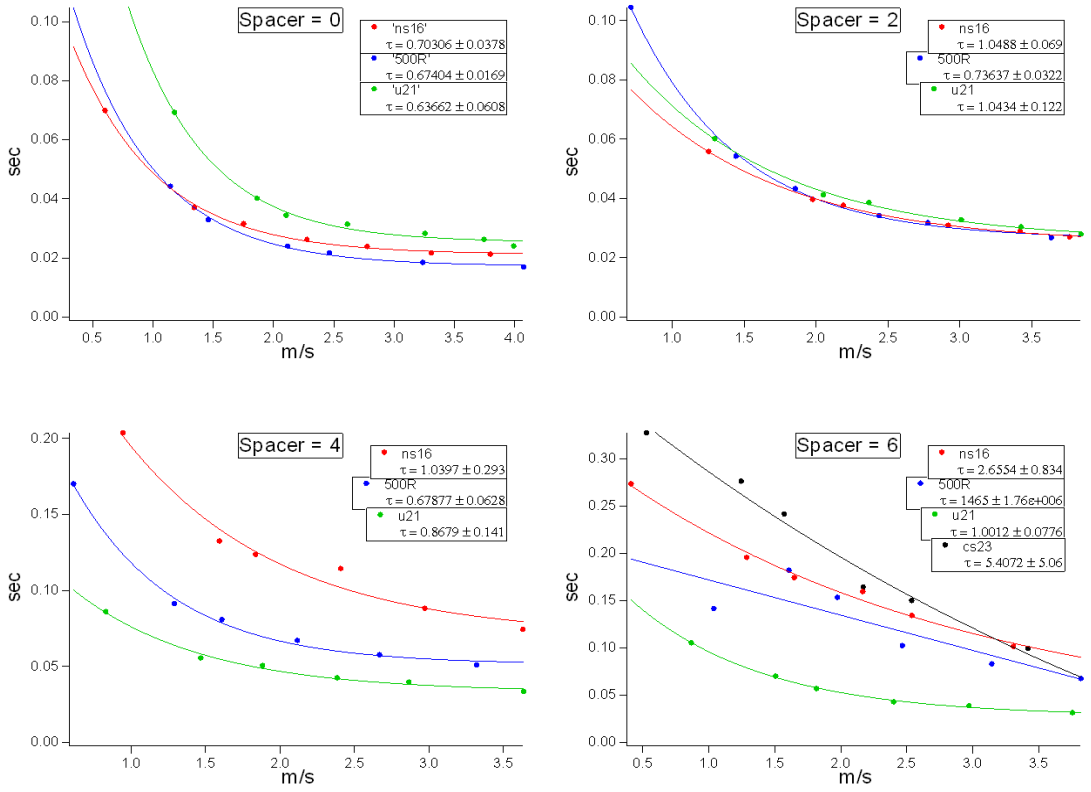

Figure 4.10 Exponential offset fits of Relaxation Time comparisons across tangential speeds.

5. Discussion

All the measures taken to reduce the noise did not truly eliminate the 60 Hz signal but the SNR was sufficient for data analysis. A digital filter could be applied to the data for smoothing, but the signal would incur small losses to the impulse responses. Since the impulses are the points of interest, all the processing was done without filtering.

The AR data set for the six spacer setting shows that cs23 is clearly very sensitive to smaller fields. This means the GUITAR coating is a definite factor in small field sensitivity. Further investigation including CS-like samples with other spacer settings would be very enlightening. If GUITAR is deemed too large of a factor in the AR, it may be beneficial to take measurements using a different conductive coating. To make working with cs23 less difficult, it may be beneficial to roughen the quartz substrate before GUITAR is deposited. This would make the measurement probes less likely to slide and scratch the surface with GUITAR coating. Additionally, it would be interesting to compare AR vs. the separation distance for the same tangential velocities, but this measurement method does not provide a consistent enough tangential speed to compare across spacer separations. In the future, it would be advantageous to set up a frequency measurement so the variac can be adjusted for specific frequency as opposed to the applied voltage. Another method to achieve a more quantifiable and increased tangential speed would be to use an AC magnetic field. This would require drastic changes to the experimental set up, but could greatly increase the resolution of the impulse separations.

In the AR data, a sharp decrease in the AR can be seen for ns16 at the zero spacer separation at ~3.9 m/s tangential speed. This hints at the possibility of a critical frequency, but is most likely due to degradation of the electrical connection between the sample and the probe over time. Further investigation into this can include increased resolution in tangential speed, as stated previously.

One glaring parameter that can affect most of the data is the tangential speed of the samples. In all the data presented here, the tangential speed barely exceeded 4 m/s. According to the data, this had little to no impact on the AR, background current, and interference with the individual current pulses. Safely increasing the tangential speed past 4 m/s or sufficiently decreasing the turn table size would provide valuable information about the

behavior of these phenomena as the time between the impulse responses or the RT decreases or vanishes.

The measurement of the RT deemed to be challenging. Due to the noisy zero current background between impulses, choosing the exact point at which the system is deemed relaxed became somewhat arbitrary and affected the accuracy of the relaxation time. This uncertainty was compounded when increasing the spacer settings which made the 6 spacer data set very noisy. However, the 0 and 2 spacer data sets fit the exponential offset line very well (figure 4.8). Comparing these two data sets, the exponential time constant (τ) appears to change with spacer setting, however, more data is needed to investigate this further. To improve the determination of the zero current background, data can be taken before inducing current in the sample. This would provide a more reliable reference for the relaxation point that can be used to measure the RT.

The tangential speeds can also greatly affect the RT measurement. As the tangential speed is increased, the time for the signal to relax between impulses also decreases. This potentially results with no zero point between impulses and eliminates the ability to measure the RT. This can be alleviated by simply increasing the size of the turn table so the system has time to relax while maintaining the same tangential speed.

In order to potentially see a difference in the signals between ns16 and and u21-type samples, the width of the mask will require thinning. This poses a challenge due to the limitations of machining as this was the smallest attainable width by the machinist (who is of highest caliber); some other mask manufacturing method will have to be used. Investigating the smallest allowable width of a sample will theoretically result in an induction limit when the sample width becomes less than the diameter of induced current loops. This could then be characterized in a similar way as a percolation threshold density.

6. Conclusion

To decrease noise in this experiment a Faraday cage, braided wires, and grounded Al foil are necessary. Data acquisition with a high sample rate such as 4800 Hz is necessary to see the resolution needed for a current impulse measurement. After processing the data it was found that samples with more nanosprings are more sensitive to smaller fields due to a large increase in surface area and that GUITAR coating also increases sensitivity to smaller fields.

A sample width of 1 mm is still above the induction threshold as there is no distinguishable difference between the response impulses of a full mat of nanosprings and the geometrically altered sample. Decreasing the sample area is necessary to probe the limits of this threshold but is met with difficulties in the machining of such small geometries.

Further investigation can be done by improving characterization of the tangential speed of the samples; using a measurement method to set a specific tangential speed of the sample would greatly increase analysis options because the samples AR could be compared categorically at the same tangential speed. Additionally, increasing the tangential speeds of the samples to the point at which the impulses interfere with one another would be very interesting.

References

Bao, Chunxiong, et al. "*In Situ* Fabrication of Highly Conductive Metal Nanowire Networks with High Transmittance from Deep-Ultraviolet to Near-Infrared." *ACS Nano*, vol. 9, no. 3, Mar. 2015, pp. 2502–09. *CrossRef*, doi:10.1021/nn504932e.

Barbero, David R., et al. "Nano-Engineering of SWNT Networks for Enhanced Charge Transport at Ultralow Nanotube Loading." *Advanced Materials*, vol. 26, no. 19, May 2014, pp. 3111–17. *CrossRef*, doi:10.1002/adma.201305843.

Cheng, I. Francis, et al. "Synthesis of Graphene Paper from Pyrolyzed Asphalt." *Carbon*, vol. 49, no. 8, July 2011, pp. 2852–61. *CrossRef*, doi:10.1016/j.carbon.2011.03.020.

Dobrokhotov, Vladimir, et al. "Toward the Nanospring-Based Artificial Olfactory System for Trace-Detection of Flammable and Explosive Vapors." *Sensors and Actuators B: Chemical*, vol. 168, June 2012, pp. 138–48. *CrossRef*, doi:10.1016/j.snb.2012.03.074.

Gao, Fan, and Zhiyong Gu. "Nano-Soldering of Magnetically Aligned Three-Dimensional Nanowire Networks." *Nanotechnology*, vol. 21, no. 11, Mar. 2010, p. 115604. *CrossRef*, doi:10.1088/0957-4484/21/11/115604.

Griffiths, David. "Electromagnetic Induction." *Introduction to Electrodynamics*, Fourth, Pearson, 2013, p. 599.

---. "The Lorentz Force Law." *Introduction to Electrodynamics*, Fourth, Pearson, 2013, p. 599.

Hass, Jamie L., et al. "Synthetic Osteogenic Extracellular Matrix Formed by Coated Silicon Dioxide Nanosprings." *Journal of Nanobiotechnology*, vol. 10, no. 1, 2012, p. 6. *CrossRef*, doi:10.1186/1477-3155-10-6.

Hu, L., et al. "Percolation in Transparent and Conducting Carbon Nanotube Networks." *Nano Letters*, vol. 4, no. 12, Dec. 2004, pp. 2513–17. *CrossRef*, doi:10.1021/nl048435y.

McIlroy, D. N., et al. "Nanosprings." *Applied Physics Letters*, vol. 79, no. 10, Sept. 2001, pp. 1540–42. *CrossRef*, doi:10.1063/1.1400079.

Schilke, Karl F., et al. "A Novel Enzymatic Microreactor with Aspergillus Oryzae β-Galactosidase Immobilized on Silicon Dioxide Nanosprings." *Biotechnology Progress*, vol. 26, no. 6, Nov. 2010, pp. 1597–605. *CrossRef*, doi:10.1002/btpr.476.

Sun, Mingming, et al. "Nano-Wire Networks of Sulfur–polypyrrole Composite Cathode Materials for Rechargeable Lithium Batteries." *Electrochemistry Communications*, vol. 10, no. 12, Dec. 2008, pp. 1819–22. *CrossRef*, doi:10.1016/j.elecom.2008.09.012.

Tan, Renwei, et al. “Electrochemical Characteristics of Nano-Graphene on a Macroporous Electrically Conductive Network Prepared by Hydrothermal Carbonization.” *Electrochimica Acta*, vol. 215, Oct. 2016, pp. 515–24. *CrossRef*, doi:10.1016/j.electacta.2016.08.144.

Ulrich, Markus, et al. “Li Ion Transport and Interface Percolation in Nano- and Microcrystalline Composites.” *Phys. Chem. Chem. Phys.*, vol. 006, no. 13, 2004, pp. 3680–83. *CrossRef*, doi:10.1039/B401895H.

Wagner, R. S., and W. C. Ellis. “Vapor-Liquid-Solid Mechanism of Single Crystal Growth.” *Applied Physics Letters*, vol. 4, no. 5, Mar. 1964, pp. 89–90. *CrossRef*, doi:10.1063/1.1753975.

Wojcik, Peter M., et al. “Nucleation, Evolution, and Growth Dynamics of Amorphous Silica Nanosprings.” *Materials Research Express*, vol. 4, no. 1, Jan. 2017, p. 015004. *CrossRef*, doi:10.1088/2053-1591/aa54dc.

Zhang, Daqing, et al. “Silicon Carbide Nanosprings.” *Nano Letters*, vol. 3, no. 7, July 2003, pp. 983–87. *CrossRef*, doi:10.1021/nl034288c.

Zulkarnain, M., et al. “Particle Dispersion Model for Predicting the Percolation Threshold of Nano-Silver Composite.” *Arabian Journal for Science and Engineering*, vol. 41, no. 6, June 2016, pp. 2363–76. *CrossRef*, doi:10.1007/s13369-015-1989-y.